Implicit-Explicit Runge-Kutta Time Integration Methods on a Spectral-Element-based Fully Compressible Non-hydrostatic Atmospheric Model

- Shin-Hoo Kang
- Tae-Jin Oh
- Hyun Nam
- Frank Giraldo

Motivation:

- KIAPS (Korea Institute of Atmospheric Prediction Systems) is aiming to build Korea's next-generation operational global NWP model by 2019
- Target: Spectral-element numerics, global resolution of 10 km and beyond, fully compressible, nonhydrostatic
- Time integration: Accurate, efficient, good parallel scalability -> HEVI
- Compare competitive TIs in the HEVI context in terms of accuracy and efficiency

Model:

NUMA 2D CG (Height based Spectral Element 2D Nonhydrostatic Model)

Applied Time Integrators:

- 1D-IMEX Additive Runge-Kutta (ARK2)
- Operator-Split RKR: Strang Carryover
- Operator-Split RKR: Ascher-Ruuth-Spiteri (2,3,3)
- Explicit SSP RK 3rd order

Note:

- Operator-Split RKR schemes treat all terms in the vertical implicit (including advection)
- For vertical implicit solver, we use GMRES

Inertia Gravity Wave Test Case

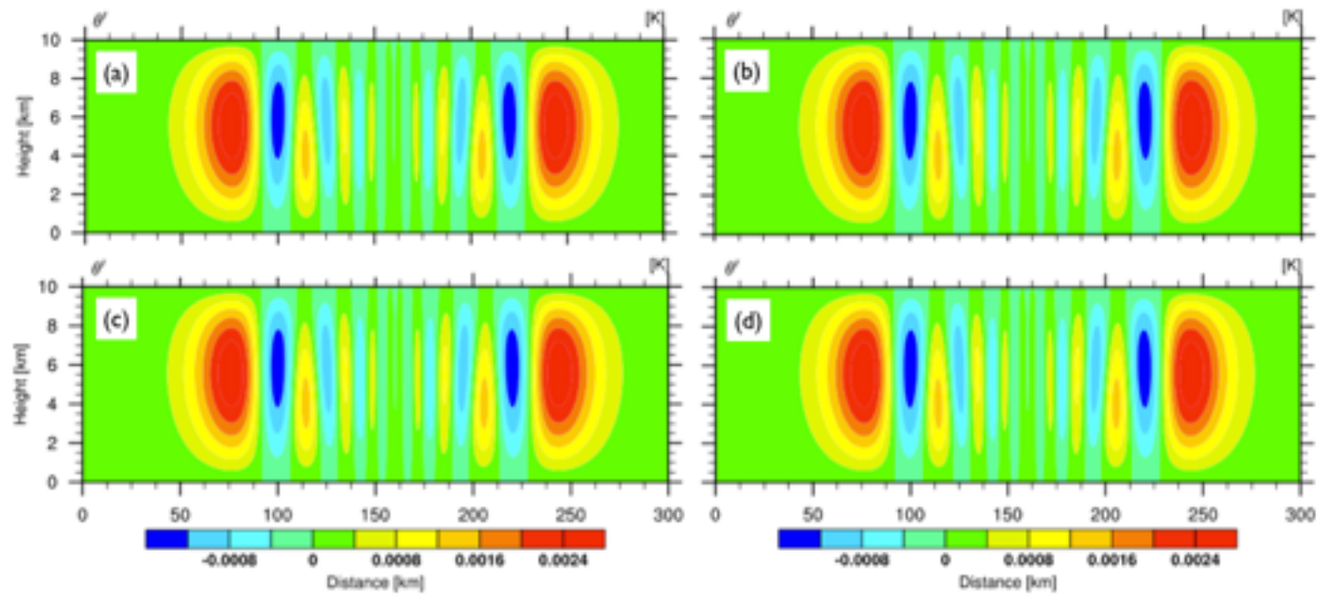

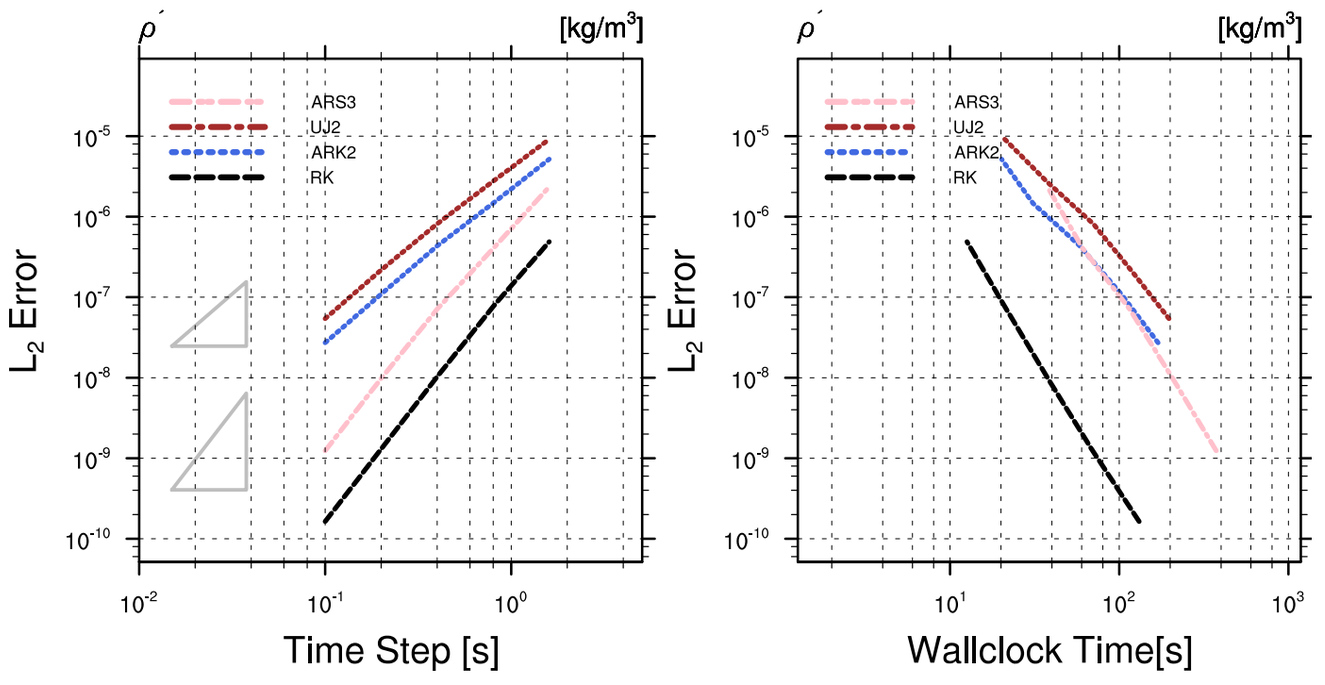

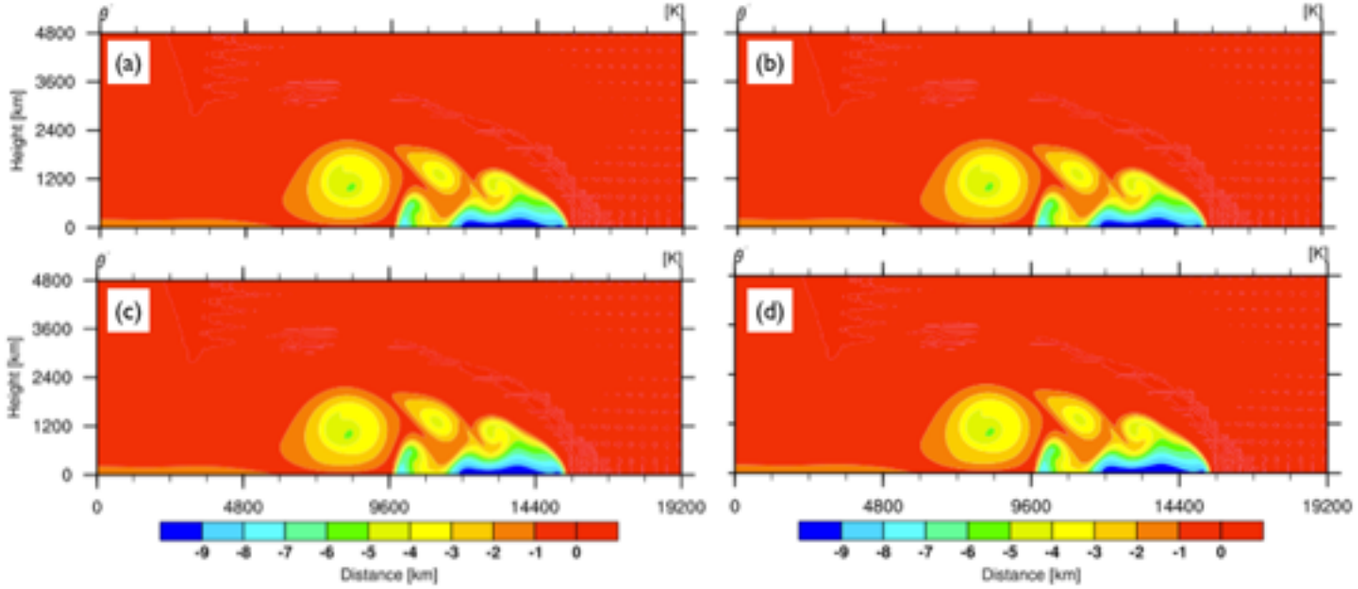
(a)
(b)
(c)
(d)
Height [km]
Distance [km]
[K]

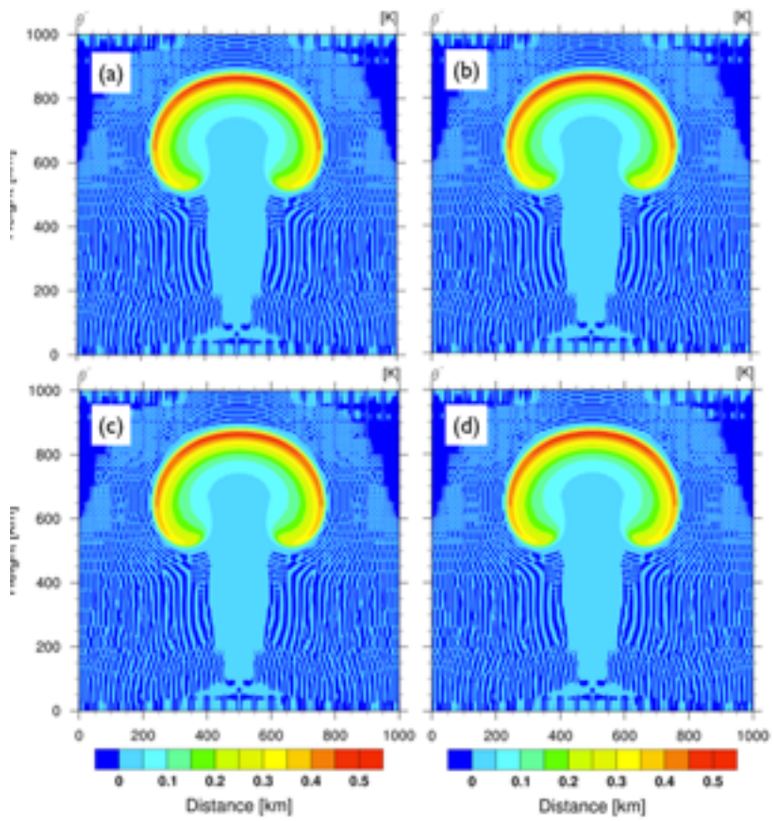
(a)
(b)
(c)
(d)
Distance [km]
[K]

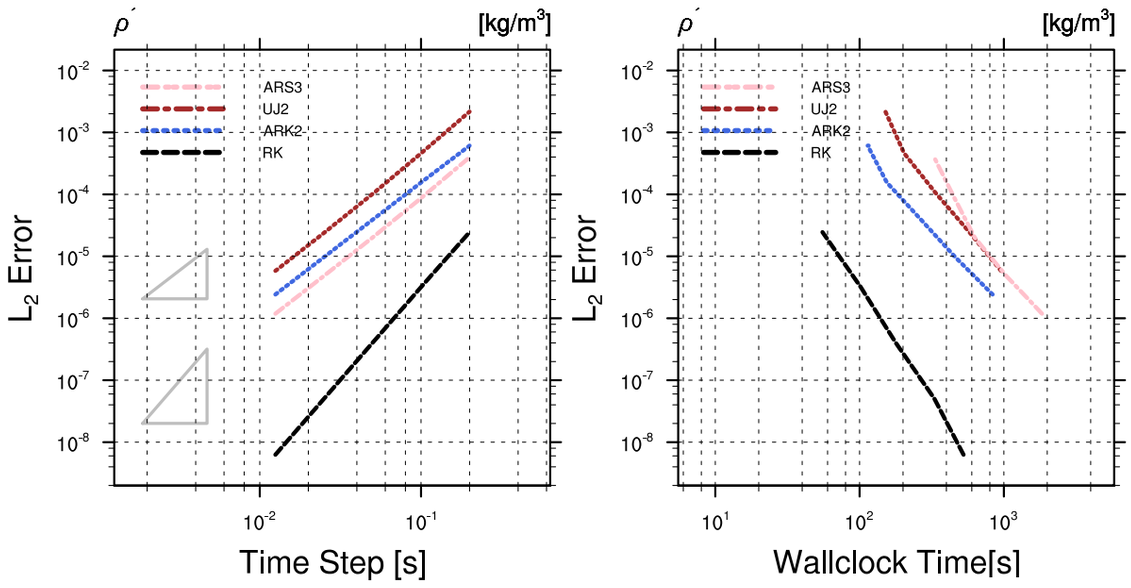
ρ´ [kg/m³]
ARS3
UJ2
ARK2
RK
L2 Error
Time Step [s]
Wallclock Time[s]

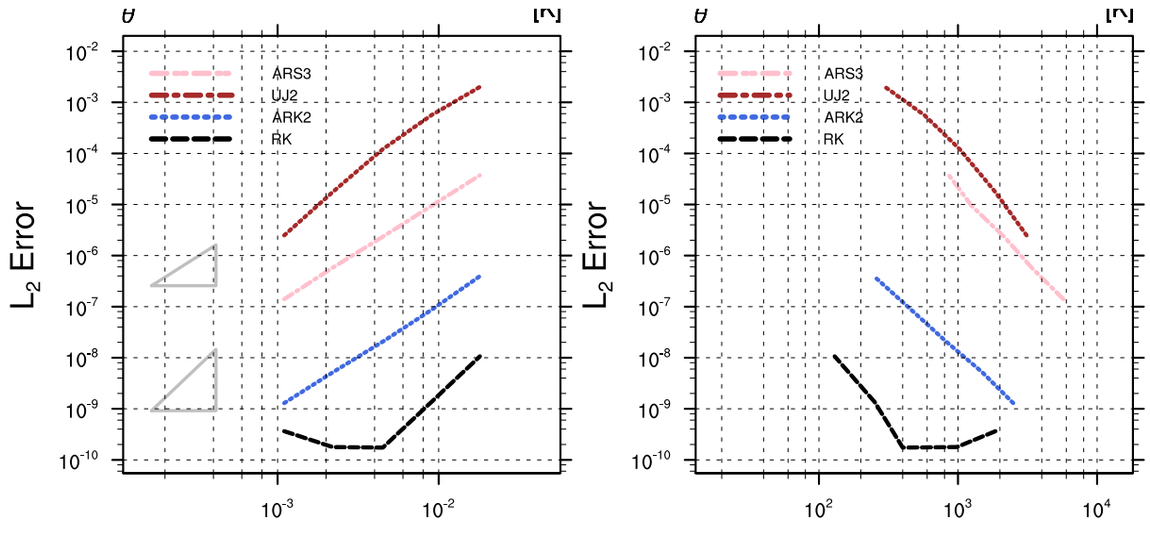
θ´ [K]
ARS3
UJ2
ARK2
RK
L2 Error

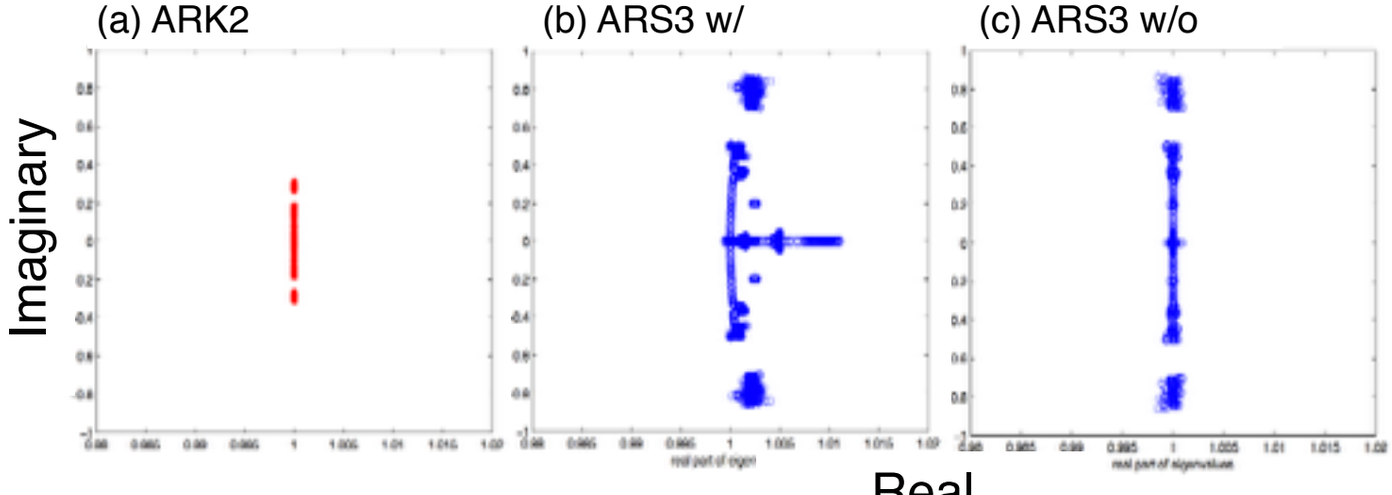
(a) ARK2
(b) ARS3 w/
(c) ARS3 w/o
Imaginary
Real

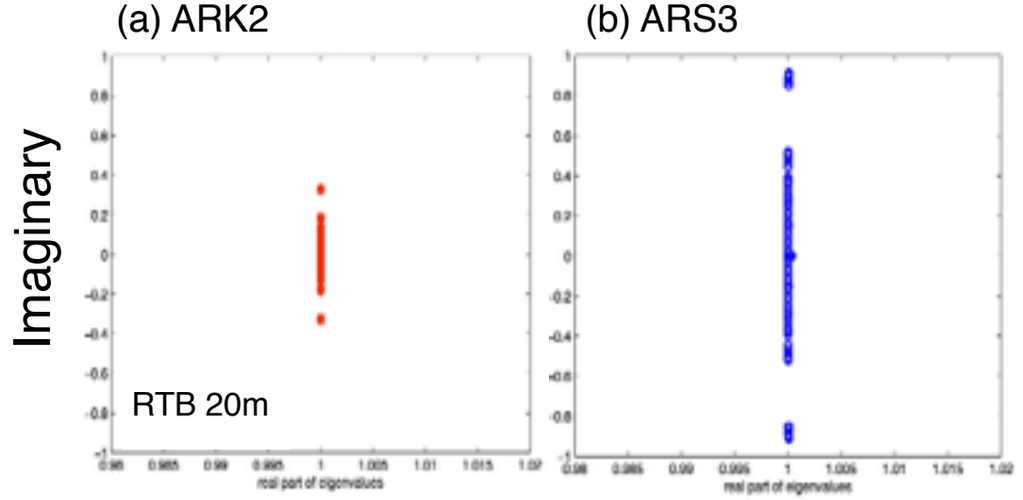
(a) ARK2
(b) ARS3
Imaginary
RTB 20m

Implicit-Explicit Runge-Kutta Time integration methods on a Spectral-Element-based Fully Compressible Non-hydrostatic Atmospheric Model

Shin-Hoo Kang[a], Tae-Jin Oh[a], Hyun Nam[a], Francis X. Giraldo[b]

[a] *Korea Institute of Atmospheric Prediction Systems (KIAPS), Seoul, Korea, sh.kang@kiaps.org,*

[b] Department of Applied Mathematics, Naval Postgraduate School, Monterey, CA, USA

Introduction

For fully compressible non-hydrostatic systems, the presence of the vertically propagating acoustic waves combined with the large aspect ratio of the horizontal and vertical grid scale makes the use of purely explicit time integrators unattractive. In order to overcome this problem, researchers have been working on soundproof governing equations or integrating the system in a 3-D semi-implicit manner. However, both methods need to solve 3-D elliptic equations which can be costly and potentially detrimental to the parallel scalability performance, especially for high resolution global models. Horizontally-Explicit Vertically-Implicit (HEVI) method is attractive in this regard considering that it overcomes the vertical CFL constraint while leaving the scalability performance intact as communications are local (Giraldo et al, 2013; Ullrich and Jablonowski, 2012; Weller et al., 2013).

In this study, four different time integrators are compared on a spectral-element-based fully compressible non-hydrostatic vertical slice model. The four time integrators are: 1) the Strang carryover scheme (Ullrich and Jablonowski 2012, hereafter UJ2) the Ascher-Ruuth-Spiteri (2, 3, 3) scheme (Ascher et al. 1997, hereafter ARS3) which are operator-split Runge-Kutta-Rosenbrock (RKR) methods, 3) 1D Implicit-Explicit Additive Runge-Kutta method (Giraldo et al., 2013, hereafter ARK2), and 4) explicit strong stability preserving Runge-Kutta method. The four methods' accuracy and efficiency are compared and analyzed for rising thermal bubble, density current, and inertia-gravity wave test cases.

Operator-Split RKR Methods

- Newton method converges quadratically, but every iteration requires Jacobian computation which is costly. Rosenbrock method restricts the Newton iteration to be performed only once which reduces the cost for computing the Jacobian. Ullrich and Jablonowski (2012) introduces UJ2 and ARS3 where both schemes are constructed with Rosenbrock steps.

UJ2

$$
\begin{aligned}
Q^{(1)} &= q^n + \frac{\triangle t}{2} q_V^n \\
Q^{(2)} &= Q^{(1)} + \triangle t R_H(Q^{(1)}) \\
Q^{(3)} &= \frac{3}{4}Q^{(1)} + \frac{1}{4}Q^{(2)} + \frac{\triangle t}{4} R_H(Q^{(2)}) \\
Q^{(4)} &= \frac{1}{3}Q^{(1)} + \frac{2}{3}Q^{(3)} + \frac{2\triangle t}{3} R_H(Q^{(3)}) \\
q_V^{n+1} &= \left[I - \frac{\triangle t}{2} \left(\frac{\partial R_V}{\partial q} \right)_{Q^{(4)}} \right]^{-1} R_V(Q^{(4)}) \\
q^{n+1} &= Q^{(4)} + \frac{\triangle t}{2} q_V^{n+1}
\end{aligned}
$$

ARS3

$$
\begin{aligned}
Q^{(1)} &= q^n + \gamma_c \triangle t R_H(q^n) \qquad \gamma_c = \frac{3+\sqrt{3}}{6} \\
q_V^{(1)} &= \left[I - \gamma_c \triangle t \left(\frac{\partial R_V}{\partial q} \right)_{Q^{(1)}} \right]^{-1} R_V(Q^{(1)}) \\
Q^{(2)} &= Q^{(1)} + \gamma_c \triangle t q_V^{(1)} \\
Q^{(3)} &= \frac{1}{\gamma_c} q^n + \left(\frac{3\gamma_c - 2}{\gamma_c} \right) Q^{(1)} + \left(\frac{1-2\gamma_c}{\gamma_c} \right) Q^{(2)} \\
&\quad + 2(1-\gamma_c)\triangle t R_H(Q^{(2)}) \\
q_V^{(2)} &= \left[I - \gamma_c \triangle t \left(\frac{\partial R_V}{\partial q} \right)_{Q^{(3)}} \right]^{-1} R_V(Q^{(3)}) \\
Q^{(4)} &= Q^{(3)} + \gamma_c \triangle t q_V^{(2)} \\
q^{n+1} &= -\frac{1}{2} q^n - \frac{3}{2}\gamma_c Q^{(1)} + \frac{3}{2} Q^{(2)} + \left(\frac{3(3\gamma_c - 2)}{2} \right) Q^{(3)} \\
&\quad + \frac{1}{2\gamma_c} Q^{(4)} + \frac{\triangle t}{2} R_H(Q^{(4)})
\end{aligned}
$$

- For each horizontal column, we compute the implicit solution for the following.

$$q_V = \sum_i^{nPoinx} q_{V,i} \qquad \left[I - \frac{\triangle t}{2} \left(\frac{\partial R_{V,i}}{\partial q_{,i}} \right)_{q^k} \right] q_{V,i} = R_{V,i}\left(q^k\right)$$

- In order to enhance computational efficiency, we utilize the Jacobian-Free Newton-Krylov (JFNK) method which only requires the Jacobian-vector product. With RKR, the Rosenbrock step is already applied and thus, Newton iteration is not required. For the Krylov solver, we use GMRES. The GMRES solver seeks the solution that minimizes the following residual.

$$residual = x - \frac{\triangle t}{2} \left(\frac{R_{V,i}(q^k + \epsilon x) - R_{V,i}(q^k)}{\epsilon} \right) - R_{V,i}\left(q^k\right)$$

- We use the following form of epsilon.

$$\epsilon = \epsilon_{jac} \sqrt{(1 + \|x\|)} \qquad \text{where} \quad \epsilon_{jac} = 10^{-6} \qquad \text{with GMRES solver tolerance } 10^{-12}$$

ARK Methods

- While the Operator-split RKR treats horizontal forcing explicitly and vertical forcing implicitly, tackling the geometrical stiffness, 1D-IMEX method identifies stiffness in terms of wave propagation speed (stiff : acoustic and gravity waves, nonstiff: advection). 1D IMEX is differentiated with 3D semi-implicit by treating only the vertical stiff terms implicitly.
- To derive 1D-IMEX method, the compact vector form of the governing equation can be written as

$$\frac{\partial \mathbf{q}}{\partial t} = [R(\mathbf{q}) - LR_V(\mathbf{q})] + LR_V(\mathbf{q}) \qquad \text{where} \qquad LR_V(\mathbf{q}) = -\begin{Bmatrix} w\frac{d\rho_o}{dz} + \rho_o \frac{dw}{dz} \\ 0 \\ \frac{1}{\rho_0}\frac{dP'}{dz} + g\frac{\rho'}{\rho_0} \\ w\frac{d\theta_o}{dz} \end{Bmatrix}$$

- Additive Runge-Kutta (ARK) methods is one of IMEX schemes. It can achieve A- and L-stability properties of arbitrary (high) order. The coefficients is proposed by Giraldo et al.(2013).

$$Q^{(i)} = q^n + \triangle t \sum_{j=1}^{i-1} a_{ij} \left[R(Q^{(j)}) - LR_V(Q^{(j)}) \right] + \triangle t \sum_{j=1}^{i} \tilde{a}_{ij} LR_V(Q^{(j)})$$

$$q^{n+1} = q^n + \triangle t \sum_{i=1}^{s} b_i \left[R(Q^{(i)}) - LR_V(Q^{(i)}) \right] + \triangle t \sum_{i=1}^{s} \tilde{b}_i LR_V(Q^{(i)})$$

Second order ARK (ARK2) method represented by Butcher Tableaux.

$$\begin{array}{c|ccc} 0 & 0 & & \\ 2-\sqrt{2} & 2-\sqrt{2} & 0 & \\ 1 & 1-\frac{1}{6}\left(3+2\sqrt{2}\right) & \frac{1}{6}\left(3+2\sqrt{2}\right) & 0 \\ \hline & \frac{1}{2\sqrt{2}} & \frac{1}{2\sqrt{2}} & 1-\frac{1}{\sqrt{2}} \end{array} \qquad \begin{array}{c|ccc} 0 & 0 & & \\ 2-\sqrt{2} & 1-\frac{1}{\sqrt{2}} & 1-\frac{1}{\sqrt{2}} & \\ 1 & \frac{1}{2\sqrt{2}} & \frac{1}{2\sqrt{2}} & 1-\frac{1}{\sqrt{2}} \\ \hline & \frac{1}{2\sqrt{2}} & \frac{1}{2\sqrt{2}} & 1-\frac{1}{\sqrt{2}} \end{array}$$

- $Q^{(i)}$ can be rewritten as $Q^{(i)} = q^n + \triangle t \sum_{j=1}^{i-1} a_{ij} R(Q^{(j)}) + \triangle t \tilde{a}_{ii} LR_V \left[\sum_{j=1}^{i-1} \left(\frac{\tilde{a}_{ij} - a_{ij}}{\tilde{a}_{ii}} \right) Q^{(j)} + Q^{(i)} \right]$

Introducing a new variable q_{tt} $\quad q_{tt} = \sum_{j=1}^{i-1} \left(\frac{\tilde{a}_{ij} - a_{ij}}{\tilde{a}_{ii}} \right) Q^{(j)} + Q^{(i)}$

gives the following linear system.

$$(I - \triangle t \tilde{a}_{ii} LR_V) q_{tt} = \hat{q} \qquad \text{where} \qquad \hat{q} = q^n + \triangle t \sum_{j=1}^{i-1} a_{ij} R(Q^{(j)}) + \sum_{j=1}^{i-1} \left(\frac{\tilde{a}_{ij} - a_{ij}}{\tilde{a}_{ii}} \right) Q^{(j)}$$

Governing Equation

- Equation set of NUMA 2D CG (Giraldo, 2013) is given as

$$\frac{\partial \rho}{\partial t} + \nabla \cdot (\rho \mathbf{u}) = 0$$

$$\frac{\partial \mathbf{u}}{\partial t} + \mathbf{u} \cdot \nabla \mathbf{u} + \frac{1}{\rho} \nabla P + g\hat{k} = \mu \nabla^2 \mathbf{u}$$

$$\frac{\partial \theta}{\partial t} + \mathbf{u} \cdot \nabla \theta = \mu \nabla^2 \theta'$$

ρ: density
$\mathbf{u}$: velocity
θ: potential temperature
P: pressure
μ: viscos coefficient
P_A: atmo. Pressure at the ground
R: universal gas constant
C_p and C_v: specific heats for constant pressure and volume
g: gravitational constant

- Splitting density, potential temperature, and pressure into hydrostatic reference values and perturbation results

$$P = P_A \left(\frac{\rho R \theta}{P_A} \right)^{\frac{C_p}{C_v}}$$

we can rewrite the governing equation as

$$\rho(\mathbf{x}, t) = \rho_o(z) + \rho(\mathbf{x}, t) \qquad \frac{dP_o}{dz} = -\rho_o g$$
$$\theta(\mathbf{x}, t) = \theta_o(z) + \theta(\mathbf{x}, t)$$
$$P(\mathbf{x}, t) = P_o(z) + P(\mathbf{x}, t)$$

- Horizontally/ Vertically decoupled system

$$\frac{\partial \rho'}{\partial t} + \mathbf{u} \cdot \nabla(\rho' + \rho_o) + (\rho' + \rho_o) \nabla \cdot \mathbf{u} = 0$$

$$\frac{\partial \mathbf{u}}{\partial t} + \mathbf{u} \cdot \nabla \mathbf{u} + \frac{1}{\rho_o + \rho'} \nabla P' + \frac{\rho' g}{\rho_o + \rho'} \hat{k} = \mu \nabla^2 \mathbf{u}$$

$$\frac{\partial \theta'}{\partial t} + \mathbf{u} \cdot \nabla(\theta' + \theta_o) = \mu \nabla^2 \theta'$$

$$\frac{\partial \mathbf{q}}{\partial t} = R_H(\mathbf{q}) + R_V(\mathbf{q}) \qquad R_H = -\begin{Bmatrix} u\frac{\partial \rho}{\partial x} + \rho \frac{\partial u}{\partial x} \\ u\frac{\partial u}{\partial x} + \frac{1}{\rho}\frac{\partial P'}{\partial x} \\ u\frac{\partial w}{\partial x} \\ u\frac{\partial \theta}{\partial x} \end{Bmatrix} + \begin{Bmatrix} 0 \\ \mu\frac{\partial^2 u}{\partial x^2} \\ \mu\frac{\partial^2 w}{\partial x^2} \\ \mu\frac{\partial^2 \theta'}{\partial x^2} \end{Bmatrix}$$

$$\mathbf{q} = \begin{Bmatrix} \rho' \\ \mathbf{u} \\ \theta' \end{Bmatrix} \qquad R_V = -\begin{Bmatrix} w\frac{\partial \rho}{\partial z} + \rho \frac{\partial w}{\partial z} \\ w\frac{\partial u}{\partial z} \\ w\frac{\partial w}{\partial z} + \frac{1}{\rho}\frac{\partial P'}{\partial z} + \frac{\rho'}{\rho} g \\ w\frac{\partial \theta}{\partial z} \end{Bmatrix} + \begin{Bmatrix} 0 \\ \mu\frac{\partial^2 u}{\partial z^2} \\ \mu\frac{\partial^2 w}{\partial z^2} \\ \mu\frac{\partial^2 \theta'}{\partial z^2} \end{Bmatrix}$$

Numerical Results

- We compared all time integrators with respect to accuracy and computational efficiency.
- For error norm calculation, we used 4th order accurate ARK4 results as our reference solution.

$$L_2 \text{ error} = \sqrt{\sum_{i=1}^{nDof} \left(q_i - q_i^{(ref)} \right)^2}$$

Inertia-Gravity wave

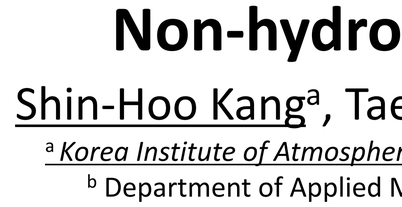

Fig. 1. Potential temperature perturbation of IG after 3000 s for 250 m resolution with 10-th order basis function polynomial. Time integration methods used are (a): RK3, (b): ARK2, (c): UJ2, and (d): ARS3

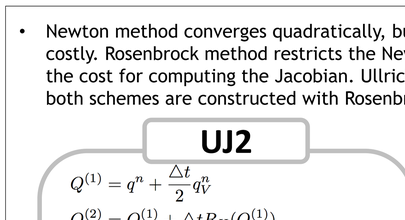

Fig. 2. Convergence rate (left) and computation efficiency results for IG. ARK2 and UJ2 shows second order accuracy, and ARS3 and RK3 are close to third order accuracy. ARK2 is more efficient than UJ2. For accuracy level between 10^{-5} to 10^{-6}, ARK2 is the most efficient, except RK.

Density Current

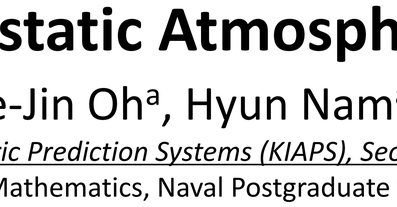

Fig. 3. Potential temperature perturbation of DC after 900 s for 50 m resolution with 8-th order polynomial. Time integration methods used are the same as Fig. 1.

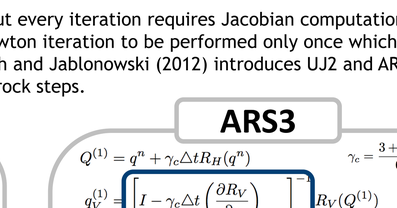

Fig. 4. Convergence rate (left) and computation efficiency results for DC. ARK2, UJ2, and ARK3 are close to second order accuracy. ARK is more efficient than UJ2 and ARS3.

Rising Thermal Bubble

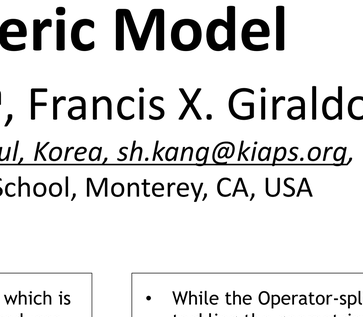

Fig. 5. Potential temperature perturbation of RTB after 540 s for 5 m resolution with 10-th order polynomial. Time integration methods used are the same as Fig. 1.

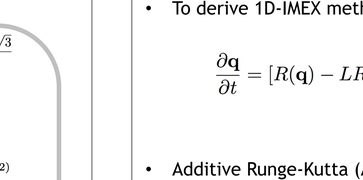

Fig. 6. . Convergence rate (left) and computation efficiency results for RTB.

- **Non-hydrostatic inertia-gravity wave test case**: Observe the evolution of a potential temperature perturbation in a channel with periodic boundary condition on the left and right. The initial perturbation propagates to the left and right symmetrically. We ran the test cases with 10th order polynomials, 250 m resolution, 0.2 s time steps for 3000 seconds. All 4 integrators show similar results (Fig. 1). RK3 and ARS3 show 3rd order convergence and ARK2 and UJ2 show 2nd order convergence as expected (Fig. 2).
- **Density current test case:** Observe the cold bubble dropped in a neutrally stratified atmosphere. The cold bubble sinks and hits the ground. Then, it creates shear as it travels along the ground generating Kelvin-Helmholtz rotors. Viscosity coefficient 75 m^2s^{-1} is applied and 8th order polynomials. 50 m resolution with 0.05 second time steps are used and the model is integrated up to 900 seconds. We can observe 3 well developed rotors for all integrators and all results look very similar. Convergence study shows that ARK2, UJ2 and ARS3 show 2nd order convergence (Fig. 4).
- **Rising thermal bubble test case**: We used 10th order polynomial with 5 m resolution, time step size of 0.0045 s and integrated up to 540 seconds. For the viscosity coefficient, we used 0.2 m^2s^{-1}. All 4 integrators show similar results (Fig. 5). RK3 shows 3rd order convergence while ARK2, UJ2, and ARS3 show 2nd order convergence (Fig. 6). Since ARS3 is only linearly 3rd order accurate, 2nd order convergence behavior is expected for ARS3 as this test case is vertically advection dominated.
- We compared the wall clock time vs L_2 error norm to assess each scheme's efficiency. For the inertia-gravity wave and rising thermal bubble test case, ARS3 is more efficient than ARK2 when L_2 error level is lower than 10^{-8}. For the density current and rising thermal bubble test case, ARK2 was the most efficient HEVI scheme.

Discussion

- The distributions of eigenvalues are examined in case of DC (Fig. 7), RTB, and IG. For all 3 cases, the eigenvalue distribution for ARK2 is bounded by 0.4 while ARS3 is bounded at 1 which is larger. We believe that the smaller eigenvalue distribution of ARK2 is driving its GMRES solution to converge faster than ARS3 and UJ2.

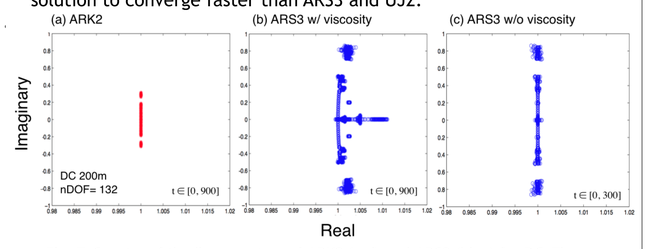

Fig. 7. Spectra of the linear system of ARK2 (red) and ARS3 (blue) for DC. The distributions of their eigenvalues are bounded by 0.4 and 1, respectively.

- A sensitivity test of GMRES solver tolerance level was performed (Fig. 8). Results indicate that ARS3 is more sensitive to the GMRES tolerance level than ARK. This indicates that we can use a larger GMRES error tolerance level for ARK which would make ARK run even faster.

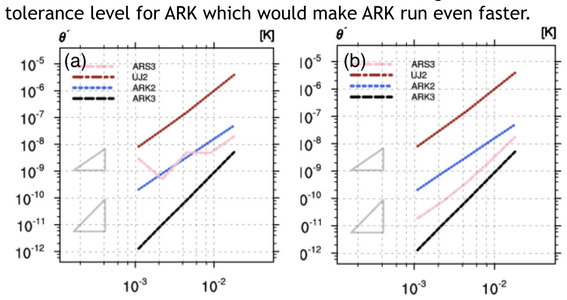

Fig. 8. A sensitivity test of GMRES solver tolerance for RTB: (a) GMRES tol=10^{-6} and (b) GMRES tol=10^{-12}

Conclusion

- For all 3 test cases, the field pattern results looked very similar for all time integrators.
- ARK2, UJ2 shows 2nd order convergence rates and ARS3 shows 3rd order for the linear problem. For DC and RTB, ARS3 showed 2nd order convergence due to the test case's inherent strong vertical advection. This is expected as ARS3 is only linearly 3rd order convergent in the vertical.
- Wallclock analysis indicates that ARK2 is more efficient that UJ2.
- Although ARK2 requires more implicit solves per timestep compared to UJ2, its smaller eigenvalue spread results in faster GMRES convergence.
- ARS3 shows strong dependency to GMRES error tolerance level while ARK2 does not. Thus, in order to achieve 3rd order convergence for ARS3, a more stringent GMRES tolerance level is needed.

References

Giraldo, F. X., J. F. Kelly, and E. M. Constantinescu, 2013: Implicit-explicit formulations of a three–dimensional nonhydrostatic unified model of the atmosphere (NUMA), *J. Sci. Comput.*, **35**, 1162-1194.

Ullrich, P. and C. Jablonowski, 2012: Operator–Split Runge-Kutta-Rosenbrock Methods for Nonhydrostatic Atmospheric Models, *Mon. Wea. Rev.*, **140**, 1257-1284.

Weller, H., S. J. Lock, and N. Wood, 2013: Runge–Kutta IMEX schemes for the Horizontally Explicit/Vertically Implicit (HEVI) solution of wave equations, *J. Comput. Phys.*, **252**, 365–381.

Knoll, D. A. and D. E. Keyes, 2004: Jacobian–free Newton-Kylov methods: a survey of approaches and applications, *J. Comput. Phys.*, **193**, 357–397.

Ascher, U., S. Ruuth, and R. Spiteri, 1997: Implicit–explicit Runge–Kutta methods for time-dependent partial differential equations, *Appl. Numer. Math.* **25**, 151–167.